Research Article Vol. 32, No. 12 / 3 Jun 2024 / Optics Express 21374

Optics EXPRESS

Real-imaginary spectrum decomposition of the transparency spectra in microwave dressed Rydberg systems

WENYU NIU,[1] LU QIN,[1,2,3,*] ZEYUN SHI,[4] YINGYING ZHANG,[1] SHIQIANG XIA,[1] XUEJING FENG,[1] QI WANG,[1] JINGXUE LIU,[1] ZHIJUN ZHAO,[5,6] ZUNLUE ZHU,[1] WEIBIN LI,[2,3] AND XINGDONG ZHAO[1,7]

[1] *School of Physics, Henan Normal University, Xinxiang, Henan 453007, China*
[2] *School of Physics and Astronomy, University of Nottingham, Nottingham NG7 2RD, United Kingdom*
[3] *Centre for the Mathematics and Theoretical Physics of Quantum Non-Equilibrium Systems, University of Nottingham, Nottingham NG7 2RD, United Kingdom*
[4] *School of Electrical and Information Engineering, Hubei University of Automotive Technology, Shiyan 442002, China*
[5] *Henan Key Laboratory of Infrared Materials & Spectrum Measures and Applications, Institute of Electromagnetic Wave, School of Physics, Henan Normal University, Xinxiang 453007, China*
[6] *zhaozhijun@htu.edu.cn*
[7] *phyzhxd@gmail.com*
[*] *qinlu@htu.edu.cn*

Abstract: To distinguish the contributions of electromagnetically induced transparency (EIT) and Autler-Townes splitting (ATS) in their applications in precision laser spectroscopy, we propose a *real-imaginary spectrum decomposition method* to investigate the transparency spectra in a four-level microwave (MW) dressed Rydberg system. We show that the opening transparency windows in the absorption spectra of probe field is a prominent character by EIT, EIT-ATS crossover, and ATS when the MW field is turned off and the intensity of the control field is adjusted. When the MW field is turned on and gradually increased, the EIT is destroyed and disappears. In addition, the most prominent characters that open a transparency window are the EIT-ATS crossover and the ATS. Then, if we further increase the intensity of the MW field, we find that the transparency windows open mainly due to the ATS. Compared to the previous considerations of this issue, which were limited to three-level systems, our four-level scheme reported here is useful for understanding the features of quantum interference in multilevel atomic systems, and has potential applications to study enhanced sensitivity, measurement spectroscopic, quantum processing, quantum communication, and transmission.

© 2024 Optica Publishing Group under the terms of the Optica Open Access Publishing Agreement

1. Introduction

Due to similar spectra being induced by different mechanisms, spectrum decomposition technology is attracting more and more attention in the field of precision measurements. For example, electromagnetically induced transparency (EIT) [1–6] and Autler-Townes splitting (ATS) [7–14] are depending on a strong control field, by which the optical absorption of a probe field in resonant atomic systems can be suppressed. Although both EIT and ATS effects can open transparency windows in probe absorption spectra, the physical mechanisms behind them are different, leading to applications in different areas [9,10]. EIT is a destructive interference phenomenon induced by two competing transition pathways and finds applications in the enhanced nonlinearity [3,15], slow light [16–18], optical soliton [19–22], optical storage [23–25], and high-precision magnetometry [26]. The ATS is a dynamical Stark shift caused by the gap between two resonances and is

#520789 https://doi.org/10.1364/OE.520789
Journal © 2024 Received 2 Feb 2024; revised 23 Mar 2024; accepted 14 May 2024; published 28 May 2024

Optics EXPRESS

related to the modification of the atomic level [10]. ATS has applications in microwave (MW) measurement, superconducting, and sensing [8,11,12,27–29].

In multilevel atomic systems, the absorption spectra between EIT and ATS appear to be similar. Hence, distinguishing between EIT and ATS poses a challenge, as the mere presence of a transparency window does not inherently elucidate whether the phenomenon corresponds to ATS or EIT. Recently, various studies have been carried out to distinguish between the EIT and ATS effects in various systems and using different methods [30–39]. In 1997, Agarwal proposed a spectrum decomposition method to analyze probe field absorption spectra of cold three-level atomic systems, theoretically distinguishing the nature of quantum interference [40]. In 2011, Anisimov *et al.* proposed the Akaike information criterion (AIC) [41] to distinguish EIT and ATS. Later, Giner *et al.* [31] carried out an experimental investigation of the transition between EIT and ATS using the method proposed by Anisimov *et al.* [41]. Subsequently, Zhu and Tan *et al.* studied the transition from EIT to ATS in different three-level atomic systems using the spectrum decomposition method [9,10,42]. Several typical three-level systems have been extensively investigated in the EIT and ATS studies. However, systematic analysis in four-level systems has been lacking. It is imperative to delineate this distinction analytically.

Moreover, much interest has been focused on the Rydberg excitation in cold and hot atomic gases, where MW dressed schemes have been widely employed to improve the sensitivity of the measurement spectroscopy [26,43–47]. Nevertheless, how to distinguish between EIT and ATS in such multilevel MW dressed schemes has not been carried out thoroughly. In addition, several experimental studies have explored ATS or EIT in molecular systems. However, observing and analyzing the spectral behaviors in these systems pose significant challenges due to the comparatively smaller transition-dipole-moment matrix elements in molecules compared to atoms, alongside the intricate vibrational and rotational energy level structures inherent to molecules. Therefore, the practical significance of studying the spectrum decomposition in multilevel systems is readily apparent.

In this work, we extend our study to a four-level system and propose *a real-imaginary spectrum decomposition method* and use the methods in Ref. [9,10,42] jointly, to investigate the transparency spectra and phase diagram for the EIT-ATS crossover in a MW dressed Rydberg system. We show that the dispersion relation depends strongly on the Rabi frequencies of control and MW fields, respectively, and we obtain the clear features of the probe field absorption spectrum and phase transition in this multilevel system through multi-dimensional adjustment. The theoretical scheme proposed here remains applicable to both atomic and molecular systems, offering a promising avenue for advancing understanding quantum interference in multilevel systems. Our results have potential applications in the study of enhanced sensitivity, measurement spectroscopy, quantum processing, quantum communication and transmission in optical systems.

2. Model

We consider a cold dilute atomic gas coupled with laser and MW fields, as shown schematically in Fig. 1(a). For suppressing the Doppler effect, the probe field and MW field propagate along the z direction and the control field propagates along counter-direction. The diagram of atomic levels is shown in Fig. 1(b). The probe field with half Rabi frequency Ω_p drives the transition from ground state $|1\rangle$ to intermediate state $|2\rangle$, and the control field with half Rabi frequency Ω_c drives the transition from intermediate state $|2\rangle$ to the Rydberg state $|3\rangle$. This ladder-type three-level atom is dressed by a MW field with half Rabi frequency Ω_m, which couples the transition between the Rydberg states $|3\rangle$ and $|4\rangle$. The total electric field $\mathbf{E}(\mathbf{r},t) = \mathbf{E}_c + \mathbf{E}_p + \mathbf{E}_m = \sum_l \mathbf{e}_l \mathcal{E}_l e^{i(\mathbf{k}_l\cdot\mathbf{r}-\omega_l t)} + \text{c.c.}$, with $\mathbf{e}_l$, $\mathcal{E}_l$, $\mathbf{k}_l$, and ω_l are the unit polarization vector, envelope, center wave vector, and center frequency of lth laser filed ($l = p, c, m$), respectively. Δ_α and Γ_α are corresponding detunings and the spontaneous emission decay rates from $|\alpha\rangle$ ($\alpha = 2, 3, 4$). So far, there are some highly sensitive detection experiments based on this system [27–29], for instance, Jing and Hu *et al.*

Optics EXPRESS

developed a novel technique for phase and frequency resolved quantum sensing of MW electric fields in experiments [26].

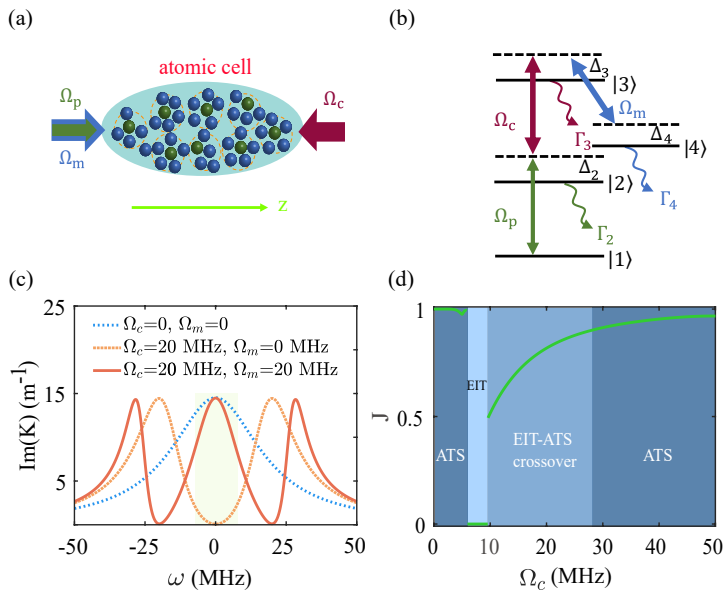

Fig. 1. (a) The Rydberg atomic cell setting, where blue and green solid balls denote atoms and Rydberg atoms, respectively. The probe and MW fields (with half Rabi frequency Ω_p and Ω_m) propagate along the z direction and the control field (half Rabi frequency Ω_c) propagates along the opposite direction. (b) MW dressed Rydberg atomic levels. The weak probe (green), strong control (red), and strong MW field (blue) with half Rabi frequencies Ω_p, Ω_c, and Ω_m drive the transitions $|1\rangle \leftrightarrow |2\rangle$, $|2\rangle \leftrightarrow |3\rangle$, and $|3\rangle \leftrightarrow |4\rangle$, respectively. States $|1\rangle$ and $|2\rangle$ are ground and excited states, respectively. States $|3\rangle$ and $|4\rangle$ are both highly excited Rydberg states. Δ_α and Γ_α are corresponding detunings and spontaneous emission decay rates from $|\alpha\rangle$ ($\alpha = 2, 3, 4$), respectively. (c) The linear absorption Im(K) as a function of frequency ω in the two-level system (dotted blue line, $\Omega_c = \Omega_m = 0$), three-level system (dash orange line, $\Omega_c = 20$ MHz and $\Omega_m = 0$), and four-level system (red solid line, $\Omega_c = \Omega_m = 20$ MHz), respectively. (d) The phase diagram of J as a function of Ω_c illustrates the transition from EIT to ATS for the four-level system with $\Omega_m = 1$ MHz. See text for details.

The dynamics of the system is described by Hamiltonian $\hat{H} = \mathcal{N}_a \int \hat{\mathcal{H}}(\mathbf{r}, \mathbf{t}) d^3\mathbf{r}$, here $\hat{\mathcal{H}}(\mathbf{r}, \mathbf{t})$ is Hamiltonian density and $\mathcal{N}_a$ is atomic density. In this work, we consider a dilute atomic gas, atomic density is relatively weak, and the Rydberg-Rydberg interaction can be neglected. Under the electric dipole and rotating-wave approximations, the Hamiltonian density is

$$\hat{\mathcal{H}} = -\hbar \sum_{\alpha=2}^{4} \Delta_\alpha \hat{S}_{\alpha\alpha} - \hbar \left(\Omega_p \hat{S}_{12} + \Omega_c \hat{S}_{23} + \Omega_m \hat{S}_{34} + \text{H.c.} \right), \tag{1}$$

here $\Delta_2 = \omega_p - (\omega_2 - \omega_1)$, $\Delta_3 = \omega_c + \omega_p - (\omega_3 - \omega_1)$, and $\Delta_4 = \omega_c + \omega_p - \omega_m - (\omega_4 - \omega_1)$. The half Rabi frequencies of the laser and MW fields are, respectively, $\Omega_p = (\mathbf{e}_p \cdot \mathbf{p}_{21}) \mathcal{E}_p / \hbar$, $\Omega_c = (\mathbf{e}_c \cdot \mathbf{p}_{32}) \mathcal{E}_c / \hbar$ and $\Omega_m = (\mathbf{e}_m \cdot \mathbf{p}_{34}) \mathcal{E}_m / \hbar$ with $\mathbf{p}_{\alpha\beta}$ the electric dipole matrix element associated with the transition between the states $|\alpha\rangle$ and $|\beta\rangle$. The time evolution of the atoms is governed by the optical Bloch equation

$$\frac{\partial \rho}{\partial t} = -\frac{i}{\hbar} \left[\hat{H}, \rho \right] - \Gamma \left[\rho \right], \tag{2}$$

Optics EXPRESS

where $\rho(\mathbf{r},t) = \langle \hat{S}(\mathbf{r},t)\rangle$ is a 4×4 density matrix describing the atomic population and coherence, Γ is a 4×4 relaxation matrix describing the spontaneous emission and dephasing. Explicit expressions of $\rho_{\alpha\beta}(\mathbf{r},t)$ are presented in Appendix A.

The motion of the probe field is described by the Maxwell equation, which under paraxial and slowly varying envelope approximations reads

$$i\left(\frac{\partial}{\partial z} + \frac{1}{c}\frac{\partial}{\partial t}\right)\Omega_p + \frac{c}{2\omega_p}\nabla_\perp^2\Omega_p + \kappa_{12}\rho_{21} = 0, \tag{3}$$

where $\nabla_\perp^2 = \partial^2/\partial x^2 + \partial^2/\partial y^2$ describes diffraction, $\kappa_{12} = \mathcal{N}_a\omega_p\left|(\mathbf{e}_p\cdot\mathbf{p}_{12})\right|^2/(2\epsilon_0 c\hbar)$ is a parameter describing the coupling between the atoms and probe field. Note that the model given above is valid also for a MW dressed Rydberg system, which can be obtained by taking $\Gamma_2 = 2\pi\times$ 6.1 MHz, $\Gamma_3 = 2\pi\times 16.7$ kHz, $\Gamma_4 = 2\pi\times 16.7$ kHz. In convenience, we assume $\Delta_2 = \Delta_3 = \Delta_4 = 0$.

3. Real-imaginary spectrum decomposition method

According to Bloch Eq. (2) and Maxwell Eq. (3), we can get dispersion relation $\mathrm{K}(\omega)$

$$\mathrm{K}(\omega) = \frac{\omega}{c} - \kappa_{12}\frac{(\omega+d_{31})(\omega+d_{41}) - |\Omega_m|^2}{(\omega+d_{21})|\Omega_m|^2 + (\omega+d_{41})|\Omega_c|^2 - (\omega+d_{21})(\omega+d_{31})(\omega+d_{41})}. \tag{4}$$

The absorption of the probe field is determined by the imaginary part of $\mathrm{K}(\omega)$, while the real part gives the dispersion. From the Eq. (4), the dispersion relation depends on two laser fields. The first is the ac Stark effect induced by the control field, reflected in the denominator, corresponding to the appearance of dressed states out of states $|2\rangle$ and $|3\rangle$, by which two Lorentzian peaks in the probe field absorption spectrum are shifted from the central frequency. The second ac Stark effect induced by the MW field, reflected in both the numerator and denominator, corresponding to the appearance of dressed states out of states $|3\rangle$ and $|4\rangle$, by which a new Lorentzian peak in the probe field absorption spectrum occurs in the central frequency.

To verify the dependence, we show numerical results in Fig. 1(c), the linear absorption Im(K) as a function of frequency ω. When $\Omega_c = \Omega_m = 0$, the atom is a two-level system. An absorption peak is visible at the central frequency (i.e., $\omega = 0$) as shown by dotted blue line. When $\Omega_c = 20$ MHz and $\Omega_m = 0$, the atom is a three-level system. Transparency window is found at the central frequency and two absorption peaks are visible at $\omega = \pm\Omega_c$ as shown by dashed orange line. When $\Omega_c = \Omega_m = 20$ MHz, two transparency windows are found at $\omega = \pm\Omega_m$ and three absorption peaks are visible at $\omega = 0, \pm\sqrt{\Omega_c^2 + \Omega_m^2}$ as shown by the solid red line [48].

Therefore, the dispersion relation strongly depends on the intensity of control and MW fields (i.e., Ω_c and Ω_m). Figure 2(a) and (b) show the numerical results of Im(K) as a function of Ω_c and Ω_m, respectively. We see that Im(K) undergoes a transition from a single absorption peak to a deep transparency window when Ω_c changes from 0 to 16 MHz with $\Omega_m = 0$. Additionally, we see that Im(K) undergoes a transition from a deep transparency window to two deep transparency windows when Ω_m changes from 0 to 16 MHz with $\Omega_c = 16$ MHz. Figure 1(c) and Fig. 2 are obtained from numerical calculations. To obtain analytical insights, we use the methods in Ref. [9,10,42] jointly, i.e. real-imaginary spectrum decomposition method. We find that the dispersion relation Eq. (4) is long and complicated. In order to analyze the quantum interference effect, the expression of dispersion relation Eq. (4) can be decomposed [10]. The second term in Eq. (4) can be written as three parts

$$\mathrm{K}(\omega) = \frac{\omega}{c} + \kappa_{12}\left[\frac{A_1}{(\omega-\omega_1)} + \frac{A_2}{(\omega-\omega_2)} + \frac{A_3}{(\omega-\omega_3)}\right], \tag{5}$$

where $A_j = \mathcal{A}_j + i\mathcal{B}_j$ ($j = 1, 2, 3$), $\mathcal{A}_j$ and $\mathcal{B}_j$ are the real and imaginary part of A_j. ω_j are three spectrum poles of $\mathrm{K}(\omega)$. The explicit expressions are given in Appendix B.

Optics EXPRESS

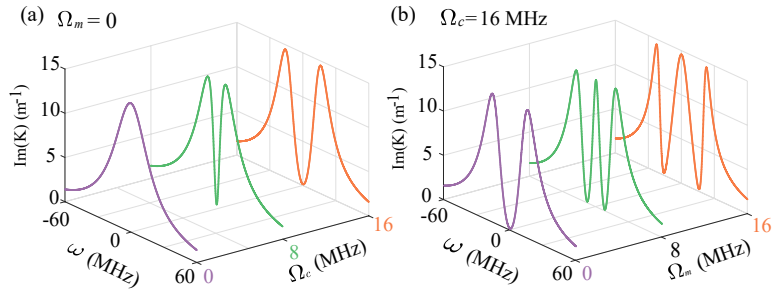

Fig. 2. The absorption spectrum of probe field Im(K) as a function of ω. (a) The absorption spectrum of three-level system have a transition from a single absorption peak to a deep transparency window when Ω_c changes from 0 to 16 MHz with $\Omega_m = 0$. (b) The absorption spectrum of the MW dressed Rydberg system have a transition from a deep transparency window to two deep transparency windows when Ω_m changes from 0 to 16 MHz with $\Omega_c = 16$ MHz.

Now, we turn to consider the quantum interference character. In the weak control field region, we can get the coefficient of Eq. (5), leading to an analytical expression,

$$\mathrm{Im(K)} = \kappa_{12}\left[\frac{\mathrm{B}_1}{\omega^2+\mathrm{W}_1^2}+\frac{\mathrm{B}_2}{\omega^2+\mathrm{W}_2^2}+\frac{\mathrm{B}_3}{\omega^2+\mathrm{W}_3^2}\right] \equiv \mathrm{L}_1+\mathrm{L}_2+\mathrm{L}_3. \tag{6}$$

In the other control field region, an analytical, but complicated expression can be obtained, too

$$\begin{aligned}\mathrm{Im(K)} &= \kappa_{12}\left\{\left[\frac{\mathcal{A}_1 W_1}{(\omega-\delta)^2+W_1^2}+\frac{\mathcal{A}_2 W_1}{(\omega+\delta)^2+W_1^2}+\frac{\mathcal{A}_3 W_3}{\omega^2+W_3^2}\right]+\left[\frac{\mathcal{B}_1(\omega-\delta)}{(\omega-\delta)^2+W_1^2}+\frac{\mathcal{B}_2(\omega+\delta)}{(\omega+\delta)^2+W_1^2}\right]\right\}\\ &\equiv L_{\mathrm{Lontz}}+L_{\mathrm{Inter}},\end{aligned} \tag{7}$$

with $W_j = \mathrm{Im}[\omega_j]$, $B_j = \mathcal{A}_j W_j$, $L_j = \kappa_{12} B_j/\left(\omega^2+W_j^2\right)$, $\delta_j = \mathrm{Re}[\omega_j]$, and $\delta_{1,2} = \pm\delta$. In the Eq. (7), B_1 and B_3 are real positive values, and B_2 is real negative value. The probe-field absorption profile comprises three Lorentzians centered at the central frequency ($\omega = 0$), one broad positive (L_1), one narrow positive (L_3), and the other narrow negative (L_2). Hence, weak control induced transparency, where EIT dominates, has a transparency window without splitting [9,10,41,42]. In the Eq. (7), the first three terms contribute from two equidistant Lorentzians, shifted from the central frequency by $\pm\delta$, and a Lorentzian at the central frequency, denoted as L_{Lontz}. While the last two terms, $\mathcal{B}_1$ and $\mathcal{B}_2$ possess opposite values, originating from the quantum destructive interference effect, represented by the interference term L_{Inter} [9,10,42]. Details of the calculation are given in Appendix B.

3.1. Applied to three-level systems

In order to verify the feasibility of our decomposition method, we first analyze the quantum interference in the absence of MW field, i.e., $\Omega_m = 0$, then the system successfully degenerates into a three-level system where the characteristics of spectra have been widely studied [10]. In this condition, $A_3 = \omega_3 = 0$ induced $B_3 = \delta_3 = 0$. To illustrate the quantum interference effect clearly, we divide Im(K) for different intensity of control field Ω_c.

In the **weak control field region** (Ω_c<Ω_{ref}), the coefficients of Eq. (6) $B_{1,2}$ are both real numbers, and $\omega_{1,2}$ are pure imaginary numbers. Here Ω_{ref} is a reference value of intensity of control field, $\Omega_{\mathrm{ref}} = |\gamma_{21} - \gamma_{31}|/2 = 9.55$ MHz (see Appendix B). Therefore, the probe field absorption comprises two Lorentzians centered at $\omega = 0$ shown in Fig. 3(a). There are a positive

Optics EXPRESS

(L_1, dotted green line) and a negative single peak (L_2, dashed-dotted blue line). Other one is a zero flat band (L_3, dots on solid blue line) because the MW field is turned off. The superposition of L_1 and L_2 give Im(K) (the solid red line), which displays two absorption peaks with a transparency window near $\omega = 0$. Due to the destructive interference between the positive L_1 and the negative L_2 in the probe field absorption spectrum, the phenomenon found here belongs to EIT based on the criterion given in [9,10].

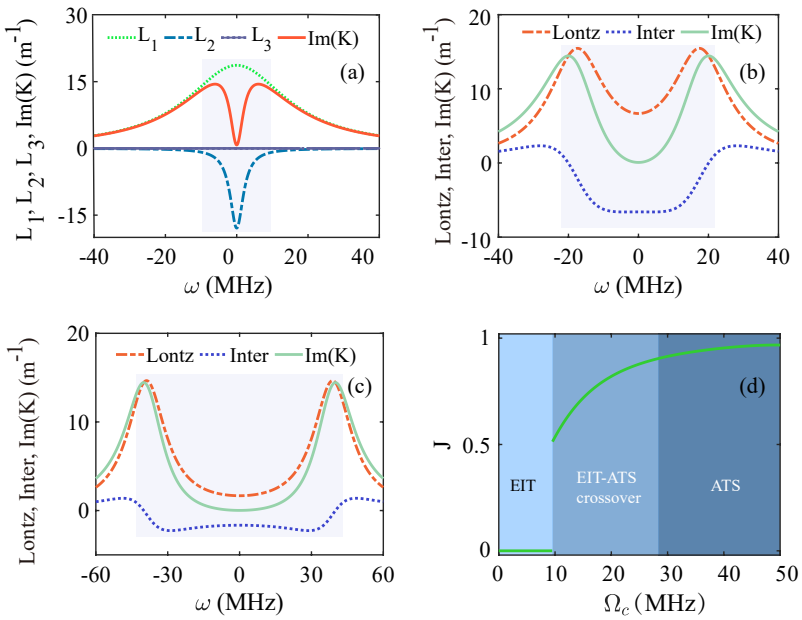

Fig. 3. The spectrum decomposition in three-level system without MW field. (a) Weak control field region with $\Omega_c = 7$ MHz$<\Omega_{\rm ref}$. There are a positive (L_1, dotted green line), a negative single peak (L_2, dashed-dotted blue line), and a zero flat band (L_3, dots on solid blue line). The superposition of L_1 and L_2 give Im(K) (the solid red line). (b) Intermediate control field region with $\Omega_c = 20$ MHz$>\Omega_{\rm ref}$, absorption spectrum contributed by Lorentzian ($L_{\rm Lontz}$, dotted-dashed red line) and destructive interference terms ($L_{\rm Inter}$, dotted blue line). The superposition of Lorentzian and destructive interference give Im(K) (the solid green line). (c) The same as (b) but for strong control field region, $\Omega_c = 40$ MHz$\gg \Omega_{\rm ref}$. (d) The phase diagram of J as a function of Ω_c illustrates the transition from EIT to ATS for the three-level system.

Figure 3(b) shows Im(K) in the **intermediate control field region**, where $\Omega_c = 20$ MHz is larger than $\Omega_{\rm ref} = 9.55$ MHz. As the control field strength increases, the values $\mathcal{B}_j$ and $\mathcal{A}_j$ are comparable [in Eq. (7)]. Hence, the absorption spectrum is jointly determined by both $L_{\rm Inter}$ and $L_{\rm Lontz}$. The dotted-dashed red line represents the contribution by the two positive Lorentzians ($L_{\rm Lontz}$), and the dotted blue line represents the negative interference term ($L_{\rm Inter}$). The sum of the positive two Lorentzians and the destructive interference constitute the absorption spectrum [Im(K), solid green line]. In this region, a large deep and wider transparency window appears in Im(K) due to the combined effect of EIT and ATS. Such a phenomenon is attributed to EIT and ATS, and is called EIT-ATS crossover.

Figure 3(c) illustrates Im(K) in the **strong control field region**, where $\Omega_c = 40$ MHz $\gg \Omega_{\rm ref}$. Continuously increasing the control filed, the values $\mathcal{B}_j$ become gradually smaller than $\mathcal{A}_j$ [in Eq. (7)]. Eventually, with a sufficiently strong control filed, the contributions from $L_{\rm Inter}$ become negligible. Hence, the opening of the transparency window is mainly due to the contribution of

Optics EXPRESS

the two Lorentzians in this region. Therefore, the phenomenon found in this case belongs to the ATS.

The above results show that the probe field absorption spectrum experiences a transition from EIT to ATS as the control field changes from small to large values. We can distinguish the EIT regions due to the destructive interference between positive and the negative Lorentzians in the probe field absorption spectrum. It is known that it's difficult to distinguish the boundary between the EIT-ATS crossover and the ATS regions. Therefore we define overlap integral of the Lorentzians and absorption spectrum Im(K), which is called the shape similarity J. A similar definition is widely used in the study of the fidelity of optical memory in atomic ensembles, coherence in quantum optics, and waveshape fidelity in optical cloning [24,49,50].

$$\mathrm{J} = \frac{|\int_{-\infty}^{\infty} L_{\mathrm{Lontz}} \cdot \mathrm{Im(K)} d\omega|^2}{\int_{-\infty}^{\infty} |L_{\mathrm{Lontz}}|^2 d\omega \cdot \int_{-\infty}^{\infty} |\mathrm{Im(K)}|^2 d\omega}. \tag{8}$$

Comparing the overlap between Lorentzians and absorption spectrum Im(K), we define J = 0 as the boundary between EIT and EIT-ATS crossover, and J = 0.9 as the boundary between EIT-ATS crossover and ATS because of the shape similarity between ATS effect and absorption spectrum almost identical, akin to the alternative definition $\mathrm{Im}(K)_{\omega=0}/\mathrm{Im}(K)_{\max} = 0.01$ as the border between EIT-ATS crossover and ATS regions [9,10,42].

Figure 3(d) shows the phase diagram of shape similarity J as a function of Ω_c illustrates the transition from EIT to ATS for the three-level ladder type system as a function of Ω_c for Ω_m=0. We distinguish three different regions, the EIT region (Ω_c<9.55 MHz), EIT-ATS crossover region ($\Omega_c \in [9.55, 27.7]$ MHz), and ATS region (Ω_c>27.7 MHz).

3.2. Applied to four-level systems

In this part, we focus on the MW dressed four-level Rydberg system, which significantly differs from the three-level situation in that the quantum interference character depends on two factors Ω_c and Ω_m, simultaneously. Due to the appearance of a MW field, the system can exhibit very different quantum interference characters that are not present for three-level atomic system. To illustrate the quantum interference characters clearly, we decompose the absorption spectrum Im(K) for different Ω_c (the relatively weak, weak, intermediate, and strong control filed regions) with fixed Ω_m. We consider a weak MW field (Ω_m = 1 MHz), firstly, and change the control field from the weak to the strong region. When the control field is relatively weak (Ω_c = 4 MHz), there are two narrow transparency windows as shown in Fig. 4(a). The dotted-dashed red line denotes the contribution from the three positive Lorentzians (L_{Lontz}), and the dashed blue line denotes a small positive interference term (L_{Inter}). The sum of the Lorentzians and the positive interference constitute the absorption spectrum [Im(K), solid green line]. We find the positive interference increases the absorption peak at the $\omega = 0$. Obviously, the opening of the transparency window is mainly due to the contribution of the three Lorentzians. Therefore, the phenomenon found in this case belongs to the ATS.

Increasing the control field to Ω_c = 7 MHz, the coefficient of Eq. (6) B_j are real numbers and ω_j are pure imaginary numbers. Therefore, the probe field absorption comprises three Lorentzians centered at $\omega = 0$ shown in Fig. 4(b). There are two positive single peak (L_1 and L_3). The other one is a negative single peak (L_2). The superposition of L_1, L_2, and L_3 give Im(K) (the solid red line), which displays three absorption peaks with two transparency windows near $\omega = \pm\Omega_m$. Because of the destructive interference between the positive $L_{1,3}$ and negative L_2 in the probe field absorption spectrum, the phenomenon found here belongs to the EIT.

Figure 4(c) shows Im(K) in the intermediate control field region, i.e., Ω_c = 20 MHz. The sum of the positive three Lorentzians and the destructive interference constitute the absorption spectrum Im(K). In this region, two large deep and wider transparency windows appear in Im(K)

Optics EXPRESS

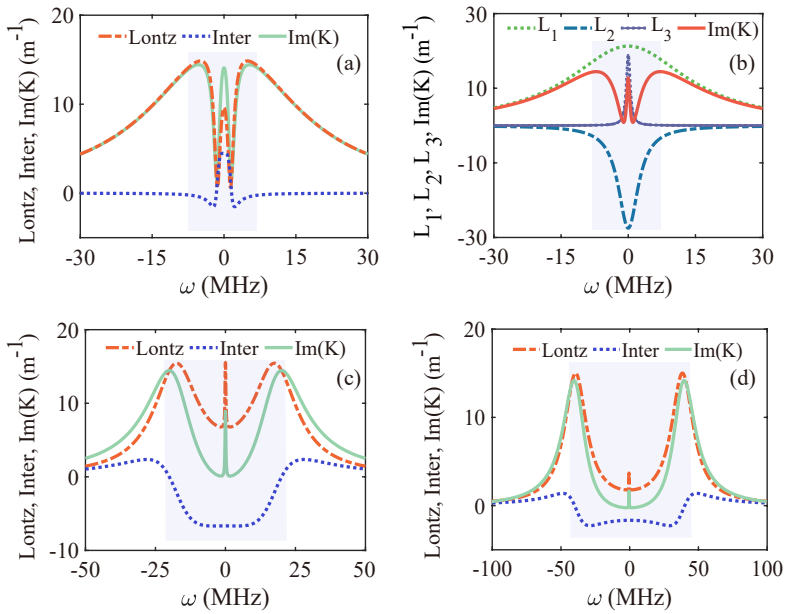

Fig. 4. The spectrum decomposition in the four-level MW dressed Rydberg system with Ω_m=1 MHz. The same as Fig. 3, but MW field is turned on. (a) The relatively weak control field region, Ω_c = 4 MHz. (b) Weak control field region, Ω_c = 7 MHz. (c) and (d) The same as (a) but for intermediate control field (Ω_c = 20 MHz) and strong control field regions (Ω_c = 40 MHz), respectively.

due to the combined effect of EIT and ATS. Such a phenomenon is attributed to the EIT-ATS crossover.

Figure 4(d) illustrates Im(K) in the strong control field region, i.e., Ω_c = 40 MHz. We find the negative interference is decrease with the increase of Ω_c that we can neglect. Therefore, the transparency window opens mainly due to the contribution of the three Lorentzians in this region. Hence, the phenomenon found in this case belongs to the ATS.

The above results show that the probe field absorption spectrum experiences a transition from ATS to EIT to EIT-ATS crossover to ATS with increasing control field. Figure 1(d) shows the phase diagram of J as a function of Ω_c illustrates the transition for the four-level system with Ω_m=1 MHz. We can distinguish four different regions, where the relatively weak control region (Ω_c<6 MHz) is an ATS region, the weak control region ($\Omega_c \in [6, 9.6]$ MHz) is an EIT region, in the intermediate control field region ($\Omega_c \in [9.6, 28]$ MHz) is an EIT-ATS crossover region, and the strong control field (Ω_c>28 MHz) is an ATS region. We see that there exists an interval in the intensity of control field ($\Omega_c \in [0, 6]$ MHz), this belongs to ATS region which is totally different from the three-level system.

We now consider what will happen for the EIT-ATS crossover if we increase the intensity of MW field, by taking Ω_m = 20 MHz and other parameters the same as Fig. 4. Figure 5 (a), (b), (c) show the Lorentzians (L_{Lontz}), and destructive interference (L_{Inter}), absorption spectrum [Im(K)]. In the weak (Ω_c = 7 MHz) and strong control field (Ω_c = 40 MHz) regions, we find the opening of the transparency windows are mainly due to the contribution of the three Lorentzians shown in Fig. 5(a) and (c). Therefore, the phenomenon found in this cases belong to the ATS. In the intermediate control field region, i.e., Ω_c = 20 MHz, two large deep and wider transparency windows appear in Im(K) due to the combined effect of EIT and ATS. Such a phenomenon is attributed to the EIT-ATS crossover as shown in Fig. 5(b).

Optics EXPRESS

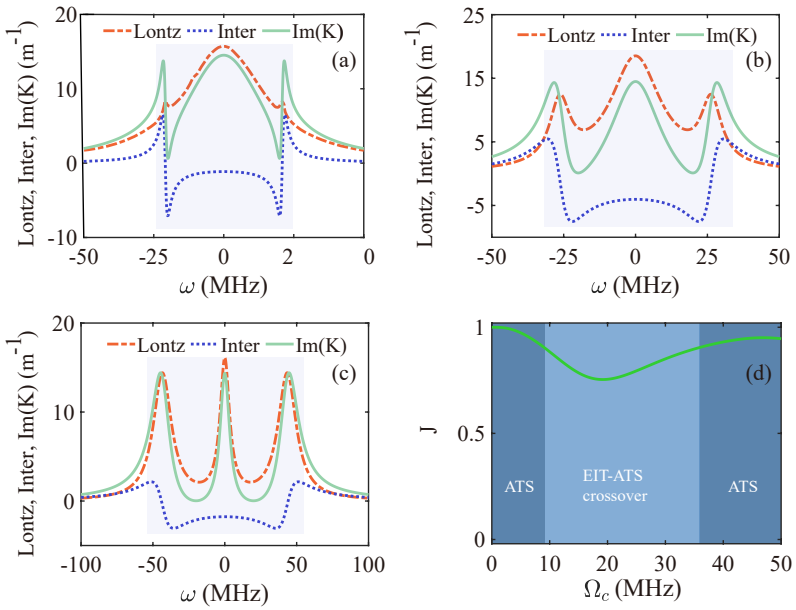

Fig. 5. The spectrum decomposition in the four-level MW dressed Rydberg system with Ω_m=20 MHz. (a), (b) and (c) The same as Fig. 4 but for weak control field Ω_c = 7 MHz, intermediate control field Ω_c = 20 MHz, and strong control field regions Ω_c = 40 MHz, respectively. (d) The phase diagram of J as a function of Ω_c illustrates the transition for the four-level system.

From Fig. 5, we see that the probe field absorption spectrum experiences a transition from ATS to EIT-ATS crossover to ATS with increasing control field. Figure 5(d) shows the phase diagram of J as a function of Ω_c illustrates the transition for the four-level system with Ω_m=20 MHz. We can distinguish three different regions, where the relatively weak and weak control regions (Ω_c<9.3 MHz) are both an ATS region, in the intermediate control field region ($\Omega_c \in [9.3, 35.4]$ MHz) is an EIT-ATS crossover region, and the strong control field (Ω_c>35.4 MHz) is an ATS region. One sees that both the relatively weak, weak, and strong control field regions are both belong to the ATS region. Comparing Fig. 1(d) and Fig. 5(d), we find that the intensity of MW field can change the phase diagram.

Further increasing the intensity of MW field (Ω_m = 40 MHz), the Lorentzians (L_{Lontz}), destructive interference (L_{Inter}), and absorption spectrum [Im(K)] are shown in the Fig. 6. In the weak (Ω_c = 7 MHz), intermediate (Ω_c = 20 MHz), and strong control field regions (Ω_c = 40 MHz), we find the transparency windows opened is mainly due to the contribution of the three Lorentzians as shown in Fig. 6(a), (b), and (c). One sees that the phenomenon found in all situations belong to ATS. The phase diagram of J as a function of Ω_c illustrates all ATS region for the four-level system with Ω_m=40 MHz can see from the dotted-dashed white line in the Fig. 6(d), the red, purple, and green stars represent Ω_c = 7, 20, 40 MHz, respectively.

From the analysis given above, we see that the probe field absorption spectrum also depends on the intensity of control and MW fields. Now, we consider the phase diagram of J as a function of Ω_c and Ω_m. In the Fig. 6(d), we find that probe field absorption spectrum experiences a transition from EIT to EIT-ATS crossover to ATS with increasing control field when MW field is switched off, i.e., Ω_m = 0. When the MW field is switched on and the intensity is weak Ω_m = 1 MHz, one sees that probe field absorption spectrum experiences a transition from ATS to EIT to EIT-ATS crossover to ATS as the control field increases. As the intensity of MW field increases, i.e.,

Optics EXPRESS

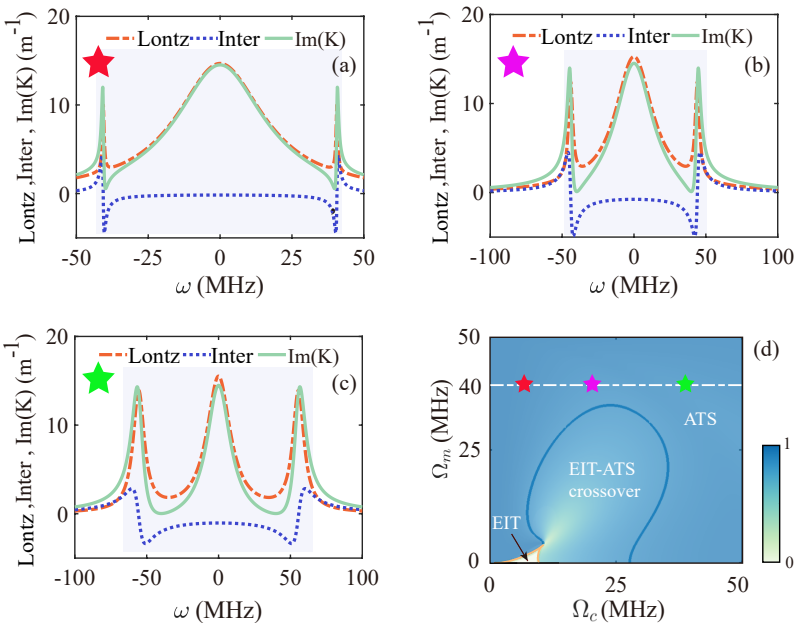

Fig. 6. The spectrum decomposition in the four-level MW dressed Rydberg system with Ω_m=40 MHz. (a), (b) and (c) The same as Fig. 4 but for weak control field Ω_c = 7 MHz, intermediate control field Ω_c = 20 MHz, and strong control field region Ω_c = 40 MHz, respectively. (d) The phase diagram of J as a function of Ω_c and Ω_m illustrates the transition from EIT to ATS for the four-level MW dressed Rydberg system. The white dotted-dashed line represent the phase diagram J as a function of Ω_c for Ω_m=40 MHz. The red, purple, and green stars represent Ω_c = 7, 20, 40 MHz, respectively. When Ω_m=40 MHz, all regions belong to ATS.

Ω_m = 20 MHz, we find that the probe field absorption spectrum experiences a transition from ATS to EIT-ATS crossover to ATS with increasing control field. When the intensity of MW field is sufficiently large, i.e., Ω_m = 40 MHz, We find that the probe field absorption spectrum all belong to ATS region and there is no transition. In Fig. 6(d), the write, blue, and light blue regions represent the EIT, ATS, and EIT-ATS crossover regions, respectively. From the results, we conclude that the EIT and ATS transitions in our system can be manipulated by tuning the intensity of the control and MW fields, leading to applications in different areas.

So far, we have applied the *real-imaginary spectrum decomposition method* to three-level and four-level atomic systems. In fact, many multilevel systems above four energy levels have been widely applied in experimental or theoretical works [50–52]. By applying a similar procedure, our method can be effectively extended to these systems.

4. Conclusion

In conclusion, we have studied real-imaginary spectrum decomposition of the transparency spectra in the MW dressed Rydberg system. We first derive the analytical expression for the dispersion spectrum of a four-level system, and then we illustrate the various mechanisms of the EIT, ATS, and their crossover in this system by comparing the three and four-level systems. We have demonstrated that both the intensity of the control and the MW fields affect the transparency window in the Rydberg atom system. When the MW field is switched off, a wide transparency window appears as the intensity of control field is increased. When the MW field is switched on, two wide transparency windows appear as the intensity of the MW field increases. The

Optics EXPRESS

EIT, ATS, and EIT-ATS crossover exist for the weak MW filed region. In the intermediate MW field region, the EIT is destroyed and the ATS and EIT-ATS crossover still exist. In the large MW field region, the EIT and EIT-ATS crossover are not possible and all cases belong to the ATS. The theoretical scheme reported here is useful for understanding the features of quantum interference in multilevel systems, and the results obtained here may have potential applications in the study of enhanced sensitivity, measurement spectroscopy, quantum processing, quantum communication and transmission.

Appendix A: Bloch equation and solutions for density-matrix element

A.1 Explicit expressions of the Bloch equation for density-matrix elements

We can obtain the explicit expression of the optical Bloch equation with the following form:

$$i\frac{\partial}{\partial t}\rho_{11} - i\Gamma_{12}\rho_{22} - \Omega_p\rho_{12} + \Omega_p^*\rho_{21} = 0, \tag{9a}$$

$$i\left(\frac{\partial}{\partial t} + \Gamma_{12}\right)\rho_{22} - i\Gamma_{23}\rho_{33} + \Omega_p\rho_{12} - \Omega_c\rho_{23} - \Omega_p^*\rho_{21} + \Omega_c^*\rho_{32} = 0, \tag{9b}$$

$$i\left(\frac{\partial}{\partial t} + \Gamma_{23}\right)\rho_{33} - i\Gamma_{34}\rho_{44} + \Omega_c\rho_{23} - \Omega_m\rho_{34} + \Omega_m^*\rho_{43} - \Omega_c^*\rho_{32} = 0, \tag{9c}$$

$$i\left(\frac{\partial}{\partial t} + \Gamma_{34}\right)\rho_{44} + \Omega_m\rho_{34} - \Omega_m^*\rho_{43} = 0, \tag{9d}$$

$$\left(i\frac{\partial}{\partial t} + d_{21}\right)\rho_{21} + \Omega_p\left(\rho_{11} - \rho_{22}\right) + \Omega_c^*\rho_{31} = 0, \tag{9e}$$

$$\left(i\frac{\partial}{\partial t} + d_{31}\right)\rho_{31} + \Omega_c\rho_{21} + \Omega_m^*\rho_{41} - \Omega_p\rho_{32} = 0, \tag{9f}$$

$$\left(i\frac{\partial}{\partial t} + d_{32}\right)\rho_{32} + \Omega_c\left(\rho_{22} - \rho_{33}\right) - \Omega_p^*\rho_{31} + \Omega_m^*\rho_{42} = 0, \tag{9g}$$

$$\left(i\frac{\partial}{\partial t} + d_{41}\right)\rho_{41} + \Omega_m\rho_{31} - \Omega_p\rho_{42} = 0, \tag{9h}$$

$$\left(i\frac{\partial}{\partial t} + d_{42}\right)\rho_{42} + \Omega_m\rho_{32} - \Omega_c\rho_{43} - \Omega_p^*\rho_{41} = 0, \tag{9i}$$

$$\left(i\frac{\partial}{\partial t} + d_{43}\right)\rho_{43} + \Omega_m\left(\rho_{33} - \rho_{44}\right) - \Omega_c^*\rho_{42} = 0. \tag{9j}$$

Here $d_{\alpha\beta} = \Delta_\alpha - \Delta_\beta + i\gamma_{\alpha\beta}$, $\gamma_{\alpha\beta} = (\Gamma_\alpha + \Gamma_\beta)/2$, $\Gamma_\beta = \sum_\alpha \Gamma_{\alpha\beta}\,(\alpha<\beta)$, $\Gamma_{\alpha\beta}$ denoting the spontaneous emission decay rate from the state $|\beta\rangle$ to the state $|\alpha\rangle$, with $\Delta_2 = \omega_p - (\omega_2 - \omega_1)$, $\Delta_3 = \omega_c + \omega_p - (\omega_3 - \omega_1)$, and $\Delta_4 = \omega_c + \omega_p - \omega_m - (\omega_4 - \omega_1)$ are the one-, two-, and three-photon detunings, respectively.

A.2 Solutions for density-matrix elements

Since the probe field is much weaker than the control and MW fields, the depletion of the atomic population in the ground state is small and a standard perturbation method can be applied to solve the system of Bloch Eq. (9). Then we can take it as a small parameter (i.e., $\Omega_p \sim \epsilon$) to make a perturbation expansion, and the population and the coherence between the states $|2\rangle$, $|3\rangle$, and

Optics EXPRESS

$|4\rangle$ are not changed. We assume $\Omega_p^{(1)}$, $\rho_{21}^{(1)}$, $\rho_{31}^{(1)}$, $\rho_{41}^{(1)} \propto \exp\{i[\mathrm{K}(\omega)z - \omega t]\}$, then get the linear solutions

$$\Omega_p^{(1)} = Fe^{i\theta}, \tag{10a}$$

$$\rho_{21}^{(1)} = -\frac{D_m}{D}Fe^{i\theta} \equiv a_{21}^{(1)}Fe^{i\theta}, \tag{10b}$$

$$\rho_{31}^{(1)} = -\frac{d_{41}\Omega_c}{D}Fe^{i\theta} \equiv a_{31}^{(1)}Fe^{i\theta}, \tag{10c}$$

$$\rho_{41}^{(1)} = \frac{\Omega_m\Omega_c}{D}Fe^{i\theta} \equiv a_{41}^{(1)}Fe^{i\theta}, \tag{10d}$$

here F is a constant, $\theta = \mathrm{K}(\omega)z - \omega t$, $D_m = (\omega + d_{31})(\omega + d_{41}) - |\Omega_m|^2$, and $D = (\omega + d_{21})D_m - (\omega + d_{41})|\Omega_c|^2$.

Appendix B: Dispersion relation

The equation of dispersion relation (4) can be written as the form

$$\mathrm{K}(\omega) = \frac{\omega}{c} - \kappa_{12}\left[\frac{(\omega + d_{31})(\omega + d_{41}) - |\Omega_m|^2}{(\omega - \omega_1)(\omega - \omega_2)(\omega - \omega_3)}\right], \tag{11}$$

with

$$\omega_1 = -\frac{b}{3} + \frac{-1 - \sqrt{3}\,\mathrm{i}}{2}\sqrt[3]{p + \sqrt{p^2 + q^3}} + \frac{-1 + \sqrt{3}\,\mathrm{i}}{2}\sqrt[3]{p - \sqrt{p^2 + q^3}} \equiv iW_1 + \delta_1, \tag{12a}$$

$$\omega_2 = -\frac{b}{3} + \frac{-1 + \sqrt{3}\,\mathrm{i}}{2}\sqrt[3]{p + \sqrt{p^2 + q^3}} + \frac{-1 - \sqrt{3}\,\mathrm{i}}{2}\sqrt[3]{p - \sqrt{p^2 + q^3}} \equiv iW_2 + \delta_2, \tag{12b}$$

$$\omega_3 = -\frac{b}{3} + \sqrt[3]{p + \sqrt{p^2 + q^3}} + \sqrt[3]{p - \sqrt{p^2 + q^3}} \equiv iW_3 + \delta_3. \tag{12c}$$

Here $p = bc/6 - b^3/27 - d/2$, $q = c/3 - b^2/9$, $b = d_{21} + d_{31} + d_{41}$, $c = d_{21}d_{31} + d_{21}d_{41} + d_{31}d_{41} - \Omega_m^2 - \Omega_c^2$, $d = d_{21}d_{31}d_{41} - \Omega_m^2 d_{21} - \Omega_c^2 d_{41}$.

B.1 Coefficient of the four level system

In order to analyze the quantum interference effect, the expression of dispersion relation Eq. (11) can be decomposed [10]. The second term of dispersion relation can be written as three parts as shown in Eq. (5). The coefficient of dispersion relation Eq. (5) can be given by

$$A_1 = -(\omega_1^2 - \Omega_m^2 + d_{31}d_{41} + d_{31}\omega_1 + d_{41}\omega_1)/[(\omega_3 - \omega_1)(\omega_2 - \omega_1)] \equiv \mathcal{A}_1 + i\mathcal{B}_1, \tag{13a}$$

$$A_2 = -(\omega_2^2 - \Omega_m^2 + d_{31}d_{41} + d_{31}\omega_2 + d_{41}\omega_2)/[(\omega_2 - \omega_3)(\omega_1 - \omega_2)] \equiv \mathcal{A}_2 + i\mathcal{B}_2, \tag{13b}$$

$$A_3 = -(\omega_3^2 - \Omega_m^2 + d_{31}d_{41} + d_{31}\omega_3 + d_{41}\omega_3)/[(\omega_3 - \omega_2)(\omega_3 - \omega_1)] \equiv \mathcal{A}_3 + i\mathcal{B}_3. \tag{13c}$$

Then the coefficients A_j of the Eq. (5) can decompose to two parts, i.e., the real ($\mathcal{A}_j$) and imaginary ($\mathrm{i}\mathcal{B}_j$) parts

$$\mathrm{Im}(\mathrm{K}) = \kappa_{12}\mathrm{Im}\left\{\left[\frac{\mathcal{A}_1}{(\omega - \omega_1)} + \frac{\mathcal{A}_2}{(\omega - \omega_2)} + \frac{\mathcal{A}_3}{(\omega - \omega_3)}\right] + \left[\frac{i\mathcal{B}_1}{(\omega - \omega_1)} + \frac{i\mathcal{B}_2}{(\omega - \omega_2)} + \frac{i\mathcal{B}_3}{(\omega - \omega_3)}\right]\right\}. \tag{14}$$

It's called the real-imaginary spectrum decomposition method.

Optics EXPRESS

In the weak control field region, we can get the coefficient of Eq. (5), where $A_{1,2,3}$ are both real numbers, and $\omega_{1,2,3}$ are pure imaginary numbers. Since $\mathrm{Re}[\omega_j] = \mathrm{Im}[A_j] = 0$ (i.e., $\delta_1 = \delta_2 = \delta_3 = \mathcal{B}_1 = \mathcal{B}_2 = \mathcal{B}_3 = 0$) in this region, we obtain

$$\begin{aligned}\mathrm{Im(K)} &= \kappa_{12}\mathrm{Im}\left[\frac{A_1}{\omega - iW_1} + \frac{A_2}{\omega - iW_2} + \frac{A_3}{\omega - iW_3}\right] \\ &= \kappa_{12}\left[\frac{B_1}{\omega^2 + W_1^2} + \frac{B_2}{\omega^2 + W_2^2} + \frac{B_3}{\omega^2 + W_3^2}\right] \equiv L_1 + L_2 + L_3,\end{aligned} \tag{15}$$

with $W_j = \mathrm{Im}[\omega_j]$, $B_j = \mathcal{A}_j W_j$, $L_j = \kappa_{12} B_j / \left(\omega^2 + W_j^2\right)$.

In the other control field region, we can get the coefficient of Eq. (5), where the imaginary part of ω_1 and ω_2 are same (i.e., $W_1 = W_2$), and the real part of ω_1 and ω_2 have opposite value (i.e. $\delta_{1,2} = \mp\delta$), and ω_3 is pure imaginary number (i.e., $\delta_3 = 0$, $\omega_3 = iW_3$). Since $\mathrm{Re}[\omega_3] = \delta_3 = 0$, $\mathrm{Im}[\mathrm{A}_3] = \mathcal{B}_3 = 0$, in the other control field region, we obtain

$$\begin{aligned}\mathrm{Im(K)} &= \kappa_{12}\mathrm{Im}\left\{\left[\frac{\mathcal{A}_1}{\omega - \omega_1} + \frac{\mathcal{A}_2}{\omega - \omega_2} + \frac{\mathcal{A}_3}{\omega - \omega_3}\right] + \left[\frac{i\mathcal{B}_1}{\omega - \omega_1} + \frac{i\mathcal{B}_2}{\omega - \omega_2} + \frac{i\mathcal{B}_3}{\omega - \omega_3}\right]\right\} \\ &= \kappa_{12}\mathrm{Im}\left\{\left[\frac{\mathcal{A}_1}{\omega + iW_1 - \delta} + \frac{\mathcal{A}_2}{\omega + iW_1 + \delta} + \frac{\mathcal{A}_3}{\omega + iW_3}\right] + \left[\frac{i\mathcal{B}_1}{\omega + iW_1 - \delta} + \frac{i\mathcal{B}_2}{\omega + iW_1 + \delta}\right]\right\} \\ &= \kappa_{12}\left\{\left[\frac{\mathcal{A}_1 W_1}{(\omega - \delta)^2 + W_1^2} + \frac{\mathcal{A}_2 W_1}{(\omega + \delta)^2 + W_1^2} + \frac{\mathcal{A}_3 W_3}{\omega^2 + W_3^2}\right] + \left[\frac{\mathcal{B}_1(\omega - \delta)}{(\omega - \delta)^2 + W_1^2} + \frac{\mathcal{B}_2(\omega + \delta)}{(\omega + \delta)^2 + W_1^2}\right]\right\} \\ &\equiv L_{\mathrm{Lontz}} + L_{\mathrm{Inter}},\end{aligned} \tag{16}$$

where the first part L_{Lontz} represents the Lorentzians distribution, and the second part L_{Inter} represents destructive interference effect.

B.2 Reduce to three level system

If we turn off the MW field, i.e., $\Omega_m = 0$, the four-level system reduce to a three-level system. The above parameters $b = d_{21} + d_{31}$, $c = d_{21}d_{31} - \Omega_c^2$, and $d = 0$. Hence, $A_3 = \omega_3 = 0$, and

$$A_{1,2} = \pm(\omega_1 + d_{31})/(\omega_1 - \omega_2), \tag{17a}$$

$$\omega_{1,2} = \frac{1}{2}\left\{-(d_{21} + d_{31}) \pm \left[4|\Omega_c|^2 + (d_{21} - d_{31})^2\right]^{1/2}\right\}. \tag{17b}$$

According to $\Delta_2 = \Delta_3 = 0$, we can simplify ω_1 and ω_2 the above equation

$$\omega_{1,2} = \frac{1}{2}\left[-i(\gamma_{21} + \gamma_{31}) \pm 2\left(|\Omega_c|^2 - \frac{|\gamma_{21} - \gamma_{31}|^2}{4}\right)^{1/2}\right]. \tag{18}$$

Obviously, when $\Omega_c \le |\gamma_{21} - \gamma_{31}|/2$, ω_1 and ω_2 are pure imaginary numbers. Hence, we can define $\mathbf{\Omega}_{\mathrm{ref}} = |\gamma_{21} - \gamma_{31}|/2$ [10].

Funding. National Natural Science Foundation of China (12074105, 12247146, 12304357).

Disclosures. The authors declare no conflicts of interest.

Data availability. Data underlying the results presented in this paper are not publicly available at this time but may be obtained from the authors upon reasonable request.

References

1. S. E. Harris, J. E. Field, and A. Imamoğlu, "Nonlinear optical processes using electromagnetically induced transparency," Phys. Rev. Lett. **64**(10), 1107–1110 (1990).

Optics EXPRESS

2. J. P. Marangos, "Electromagnetically induced transparency," J. Mod. Opt. **45**(3), 471–503 (1998).
3. M. Fleischhauer, A. Imamoglu, and J. P. Marangos, "Electromagnetically induced transparency: Optics in coherent media," Rev. Mod. Phys. **77**(2), 633–673 (2005).
4. W. Li, D. Viscor, S. Hofferberth, *et al.*, "Electromagnetically induced transparency in an entangled medium," Phys. Rev. Lett. **112**(24), 243601 (2014).
5. Q. Zhang, Z. Bai, and G. Huang, "Fast-responding property of electromagnetically induced transparency in Rydberg atoms," Phys. Rev. A **97**(4), 043821 (2018).
6. J. Malik, S. K. Oruganti, S. Song, *et al.*, "Electromagnetically induced transparency in sinusoidal modulated ring resonator," Appl. Phys. Lett. **112**(23), 234102 (2018).
7. S. H. Autler and C. H. Townes, "Stark effect in rapidly varying fields," Phys. Rev. **100**(2), 703–722 (1955).
8. R. Shimano and M. Kuwata-Gonokami, "Observation of Autler-Townes splitting of biexcitons in CuCl," Phys. Rev. Lett. **72**(4), 530–533 (1994).
9. C. Zhu, C. Tan, and G. Huang, "Crossover from electromagnetically induced transparency to Autler-Townes splitting in open V-type molecular systems," Phys. Rev. A **87**(4), 043813 (2013).
10. C. Tan and G. Huang, "Crossover from electromagnetically induced transparency to Autler-Townes splitting in open ladder systems with Doppler broadening," J. Opt. Soc. Am. B **31**(4), 704–715 (2014).
11. W. Li, J. Li, L. Yu, *et al.*, "Observation of Aulter-Townes splitting in subwavelength grating metamaterial ring resonators," APL Photonics **8**(1), 016102 (2023).
12. M. A. Sillanpää, J. Li, K. Cicak, *et al.*, "Autler-Townes effect in a superconducting three-level system," Phys. Rev. Lett. **103**(19), 193601 (2009).
13. M. T. Simons, J. A. Gordon, C. L. Holloway, *et al.*, "Using frequency detuning to improve the sensitivity of electric field measurements via electromagnetically induced transparency and Autler-Townes splitting in Rydberg atoms," Appl. Phys. Lett. **108**(17), 174101 (2016).
14. J. A. Gordon, C. L. Holloway, A. Schwarzkopf, *et al.*, "Millimeter wave detection via Autler-Townes splitting in rubidium Rydberg atoms," Appl. Phys. Lett. **105**(2), 024104 (2014).
15. Z. Bai and G. Huang, "Enhanced third-order and fifth-order Kerr nonlinearities in a cold atomic system via Rydberg-Rydberg interaction," Opt. Express **24**(5), 4442–4461 (2016).
16. C. Shou and G. Huang, "Highly efficient and controllable surface polariton beam splitters," Phys. Rev. A **100**(6), 063844 (2019).
17. C. Shou and G. Huang, "Slow-light soliton beam splitters," Phys. Rev. A **99**(4), 043821 (2019).
18. Y. Huang, C. Min, and G. Veronis, "Subwavelength slow-light waveguides based on a plasmonic analogue of electromagnetically induced transparency," Appl. Phys. Lett. **99**(14), 143117 (2011).
19. Y. Chen, Z. Bai, and G. Huang, "Ultraslow optical solitons and their storage and retrieval in an ultracold ladder-type atomic system," Phys. Rev. A **89**(2), 023835 (2014).
20. Y. Chen, Z. Chen, and G. Huang, "Storage and retrieval of vector optical solitons via double electromagnetically induced transparency," Phys. Rev. A **91**(2), 023820 (2015).
21. Y. V. Kartashov, B. A. Malomed, and L. Torner, "Solitons in nonlinear lattices," Rev. Mod. Phys. **83**(1), 247–305 (2011).
22. Y. S. Kivshar and G. P. Agrawal, *Optical solitons: From fibers to photonic crystals*, (Academic press, 2003).
23. D. F. Phillips, A. Fleischhauer, A. Mair, *et al.*, "Storage of light in atomic vapor," Phys. Rev. Lett. **86**(5), 783–786 (2001).
24. Z. Bai, W. Li, and G. Huang, "Stable single light bullets and vortices and their active control in cold Rydberg gases," Optica **6**(3), 309–317 (2019).
25. Z. Bai, Q. Zhang, and G. Huang, "Quantum reflections of nonlocal optical solitons in a cold Rydberg atomic gas," Phys. Rev. A **101**(5), 053845 (2020).
26. M. Jing, Y. Hu, J. Ma, *et al.*, "Atomic superheterodyne receiver based on microwave-dressed Rydberg spectroscopy," Nat. Phys. **16**(9), 911–915 (2020).
27. H. Fan, S. Kumar, J. Sedlacek, *et al.*, "Atom based RF electric field sensing," J. Phys. B: At. Mol. Opt. Phys. **48**(20), 202001 (2015).
28. J. A. Sedlacek, A. Schwettmann, H. Kübler, *et al.*, "Microwave electrometry with Rydberg atoms in a vapour cell using bright atomic resonances," Nat. Phys. **8**(11), 819–824 (2012).
29. Z.-K. Liu, L.-H. Zhang, B. Liu, *et al.*, "Deep learning enhanced Rydberg multifrequency microwave recognition," Nat. Commun. **13**(1), 1997 (2022).
30. P. Anisimov and O. Kocharovskaya, "Decaying-dressed-state analysis of a coherently driven three-level Λ system," J. Mod. Opt. **55**(19-20), 3159–3171 (2008).
31. L. Giner, L. Veissier, B. Sparkes, *et al.*, "Experimental investigation of the transition between Autler-Townes splitting and electromagnetically-induced-transparency models," Phys. Rev. A **87**(1), 013823 (2013).
32. C. L. Holloway, J. A. Gordon, A. Schwarzkopf, *et al.*, "Sub-wavelength imaging and field mapping via electromagnetically induced transparency and Autler-Townes splitting in Rydberg atoms," Appl. Phys. Lett. **104**(24), 244102 (2014).
33. J. Liu, H. Yang, C. Wang, *et al.*, "Experimental distinction of Autler-Townes splitting from electromagnetically induced transparency using coupled mechanical oscillators system," Sci. Rep. **6**(1), 19040 (2016).

Optics EXPRESS

34. M. Q. Ayaz, M. Waqas, S. Qamar, *et al.*, "Coherent control and storage of a microwave pulse in a one-dimensional array of artificial atoms using the Autler-Townes effect and electromagnetically induced transparency," Phys. Rev. A **97**(2), 022318 (2018).
35. S. K. Nath, V. Naik, A. Chakrabarti, *et al.*, "Discriminating electromagnetically induced transparency from Autler-Townes splitting in a ξ system," J. Opt. Soc. Am. B **36**(9), 2610–2617 (2019).
36. L. Hao, Y. Jiao, Y. Xue, *et al.*, "Transition from electromagnetically induced transparency to Autler–Townes splitting in cold cesium atoms," New J. Phys. **20**(7), 073024 (2018).
37. Z. Ji, Y. Jiao, Y. Xue, *et al.*, "Distinction of electromagnetically induced transparency and Autler-Towners splitting in a Rydberg-involved ladder-type cold atom system," Opt. Express **29**(8), 11406–11415 (2021).
38. H. Wu, Y.-P. Ruan, Z. Li, *et al.*, "Fundamental Distinction of electromagnetically induced transparency and Autler-Townes splitting in breaking the Time-Reversal Symmetry," Laser Photonics Rev. **16**(9), 2100708 (2022).
39. X.-G. Lu, X.-X. Miao, J.-H. Bai, *et al.*, "Crossover between electromagnetically induced transparency and Autler-Townes splitting with dispersion," Chin. Phys. B **24**(9), 094204 (2015).
40. G. S. Agarwal, "Nature of the quantum interference in electromagnetic-field-induced control of absorption," Phys. Rev. A **55**(3), 2467–2470 (1997).
41. P. M. Anisimov, J. P. Dowling, and B. C. Sanders, "Objectively discerning Autler-Townes splitting from electromagnetically induced transparency," Phys. Rev. Lett. **107**(16), 163604 (2011).
42. C. Tan, C. Zhu, and G. Huang, "Analytical approach on linear and nonlinear pulse propagations in an open Λ-type molecular system with doppler broadening," J. Phys. B: At. Mol. Opt. Phys. **46**(2), 025103 (2012).
43. T. F. Gallagher, *Rydberg Atoms* (Cambridge University Press, 2008), chap. 10.
44. M. Saffman, T. G. Walker, and K. Mølmer, "Quantum information with Rydberg atoms," Rev. Mod. Phys. **82**(3), 2313–2363 (2010).
45. D. Petrosyan and K. Mølmer, "Binding potentials and interaction gates between microwave-dressed Rydberg atoms," Phys. Rev. Lett. **113**(12), 123003 (2014).
46. M. Tanasittikosol, J. D. Pritchard, D. Maxwell, *et al.*, "Microwave dressing of Rydberg dark states," J. Phys. B: At. Mol. Opt. Phys. **44**(18), 184020 (2011).
47. B. J. DeSalvo, J. A. Aman, C. Gaul, *et al.*, "Rydberg-blockade effects in Autler-Townes spectra of ultracold strontium," Phys. Rev. A **93**(2), 022709 (2016).
48. Y.-L. Zhou, D. Yan, and W. Li, "Rydberg electromagnetically induced transparency and absorption of strontium triplet states in a weak microwave field," Phys. Rev. A **105**(5), 053714 (2022).
49. R. Loudon, *The quantum theory of light* (OUP Oxford, 2000), chap. 3.
50. L. Qin, C. Hang, and G. Huang, "High-fidelity and controllable cloning of high-dimensional optical beams with a Rydberg atomic gas," Phys. Rev. A **102**(6), 063707 (2020).
51. C. Hang, W. Li, and G. Huang, "Nonlinear light diffraction by electromagnetically induced gratings with $\mathcal{PT}$ symmetry in a Rydberg atomic gas," Phys. Rev. A **100**(4), 043807 (2019).
52. J. Han, T. Vogt, C. Gross, *et al.*, "Coherent microwave-to-optical conversion via six-wave mixing in Rydberg atoms," Phys. Rev. Lett. **120**(9), 093201 (2018).